Siemens Logo Here

Lehrstuhl für Hochfrequenztechnik
Technische Universität München
Prof. Dr.-Ing. Thomas Eibert

Master's Thesis

Object Classification based on Micro-Doppler Signatures

Alexis González Argüello

Munich, 17-11-2017

Faculty:	Electro- und Informationstechnik
Matriculation Number:	03640751
Reviewer:	Prof. Dr.-Ing. Thomas Eibert
Supervisor:	M. Sc. Dipl.-Ing. Dominic Berges
Beginning of the Thesis:	01-10-2017
End of the Thesis:	17-11-2017

Sperrvermerk

Declaration of Authorship

Dedicated to..

Contents

1. Introduction

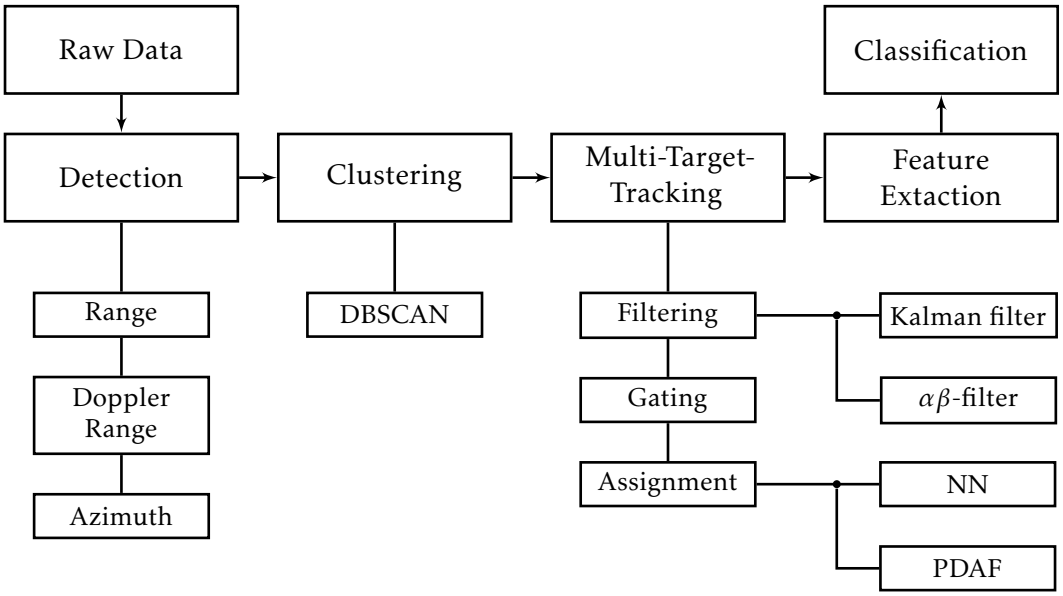

Figure 1.1.: Block Diagram of the whole process

2. Radar Fundamentals

The basic idea behind radar measurement systems is the use of electromagnetic waves to search for objects. Broadly, a modulated waveform is generated and transmitted through directive antennas. The waveform travels through space at a constant velocity (the speed of light), and reflects of any object (target) present in the measurement space. The reflected waveform is the measured and processed in order to obtain information about the present objects. This information usually includes position (range) and radial speed (Doppler), which is where the radar (RAdio Detection and Ranging) obtained its name from.

This chapter introduces basic concepts of the signal processing used on the waveform received by the radar. The reader is referred to [1] for a more detailed explanation of each of the concepts presented here. This chapter is organized as follows. The basic terminology of radars is presented in section 2.1, followed by a simple signal model presented in section 2.3, which is used to explain the signal processing steps used to estimate the range (**??**) and the radial-velocity (**??**). In order to obtain the position of the targets in Cartesian coordinates, the measurement of the angle between the target and the boresight of the radar is required. Several algorithms to calculate this angle are presented in section 2.5. Finally, the theory behind thresholding is introduced in **??**.

2.1. Radar Definitions

As already mentioned, the signal reflected from an object is measured and processed in order to obtain information about the target. This reflections are also known in literature as radar echoes. Given that electromagnetic waves travel at the speed of light, the measurement of the time the signal takes to travel from the radar to the target and back, can be used to find an estimate of the distance at which the target is present. This distance is called range R and is given by

$$R = \frac{c\Delta t}{2}, \tag{2.1}$$

where Δt is the measured time (also called delay), and c the speed of light considering the properties of the medium. The factor 1/2 takes into account that the measured delay is for the "round-trip" of the signal.

A radar either transmits (and receives) a train of pulses (pulsed radar), or emits signals with a varying frequency for a repeating period of time (continuous wave radar). For both cases, one can define the pulse repetition interval T, as the amount of time a cycle takes place, as illustrated in fig. 2.1, and the pulse repetition frequency f_r as its inverse

$$f_r = \frac{1}{T}. \tag{2.2}$$

Furthermore, the pulse-width, i.e. the time the signal is being transmitted, is denoted by τ. Depending on these parameters, the maximum unambiguous range can be found by

$$R_u = c\frac{T}{2} = \frac{c}{2f_r}. \tag{2.3}$$

As depicted in fig. 2.1, for echoes coming from targets further than R_u the return reaches the radar which such a high delay, that it can be interpreted as the return from the next pulse, leading to a false-estimation of the range. In this case, for instance a target located at $R_2 > R_u$ causes a return echo after the second pulse has already been transmitted. Here, the second pulse received by the radar can either be from the object located at R_1, which was previously measured, or the one are R_2. Therefore, objects at R_2 would wrongfully be detected as located at R_1.

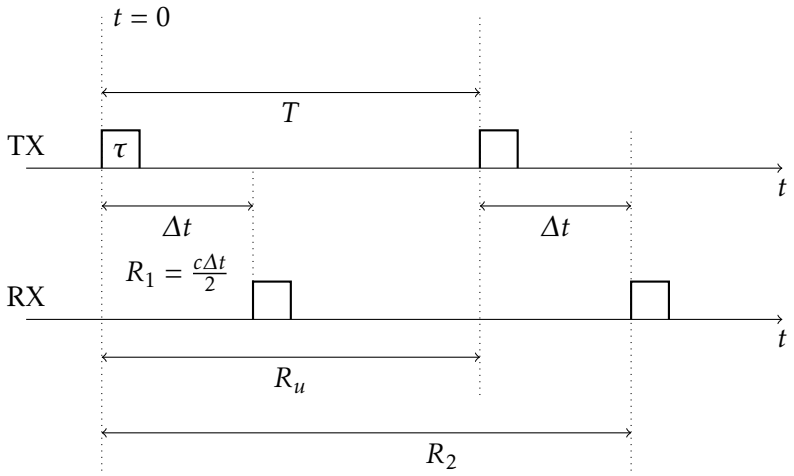

Figure 2.1.: Illustrating the unambiguous range.

On the other hand, the pulse width determines the ability of a radar to distinguish between two objects that are very close to each other. In other words, targets that are too close to each other will be "seen" as a single object by the radar. The minimal distance required for two targets to be distinguishable is called range resolution ΔR and is given by

$$\Delta R = \frac{c\tau}{2} = \frac{c}{2B}, \tag{2.4}$$

where B is the bandwidth of the radar. Usually, one divides the measurement space covered by the radar into M range bins. Where each bin corresponds to a cell of the size ΔR. The number of range bins is given by

$$M = \frac{R_{max} - R_{min}}{\Delta R}. \tag{2.5}$$

Radar echoes coming from moving targets have the characteristic of a shift in the center frequency due to the motion of the object itself. This phenomenon is known as the Doppler effect, and the shift caused by the object is

$$f_d = \frac{2v\cos\theta}{c} f_0 = \frac{2v\cos\theta}{\lambda}, \tag{2.6}$$

where θ is the angle between boresight angle of the radar and the target's velocity, $v\cos\theta$ is the radial velocity of the target, f_0 the wavelength of the waveform and λ the wavelength

$$\lambda = \frac{v}{f_0}. \tag{2.7}$$

As depicted in fig. 2.2, targets approaching to the radar can be detected by observing a positive Doppler shift f_d, while objects getting away from the radar cause a negative shift.

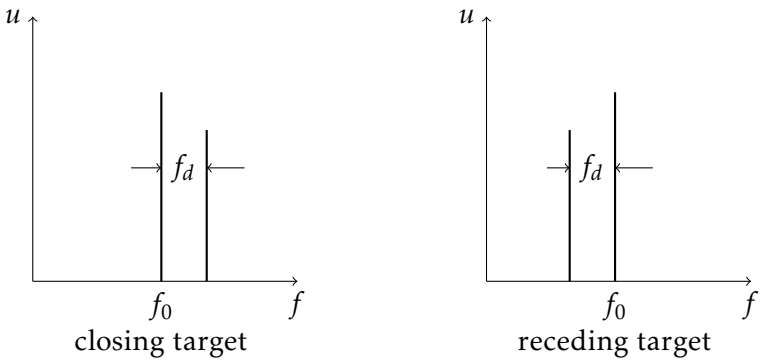

Figure 2.2.: Illustrating the Doppler frequency.

2.2. MIMO Array

For the estimation of the azimuth and elevation of a target's position, the phase array radar has been a popular choice during the past decades. This technique employs a series of antennas to transmit and receive the electromagnetic waveform before mentioned. Here, the phase of each element in the group of transmitted is adjusted for the radar to be able to suppress the response from specific directions and thus, "scan" a specific direction. The angular resolution of this method, however, strongly depends on the number of elements in the antenna array. An attractive alternative to the simple phase array is its combination with the Multiple-Input Multiple-Output (MIMO) concept [2].

As the name implies, a MIMO radar consists of multiple transmit (TX) antennas and receive (RX) antennas. M_t transmit and M_r receive elements are assumed. The difference from the phase array radar is that the signals transmitted by each of the TX elements are diversified, leading to $M_t \times M_r$ propagation channels. This, with only $M_t + M_r$ antenna elements. With this concept, a higher performance with a substantially lower cost can be achieved, which is why the MIMO array has been chosen for the purpose of this thesis.

Several methods to the define the diversity of the TX channels have been proposed, these include frequency division multiplexing, spatial coding, orthogonal waveforms and time division multiplexing. The latter has been chosen and implemented as presented in [3]. As the name indicates and as presented in fig. 2.3, the concept time division multiplexing consists in switching the transmit antenna at each consecutive pulse. Hereby, one is able to differentiate at the receiver from which TX element is the signal coming simply by looking at the time of reception, which is important for the estimation of the azimuth profile (section 2.5).

A further design concern is the array manifold. Different array forms can be found in literature, where the most common are the uniform linear array (ULA) and the uniform circular array (UCA) [4], which are depicted in figs. 2.4 and 2.5. As the name indicates, this manifolds consists of equidistant antenna elements in either linear or circular form. The MIMO-radar chosen here consists in 2 TX and 4 RX array resulting in 8 virtual channels.

If the far-field condition is satisfied, the MIMO-configuration can be modeled as an ULA of $M_t \times M_r$ virtual antennas. Given the position of the TX-elements x_i^{Tx} and RX-elements x_j^{Rx} the virtual ULA is modeled by antenna elements at

$$\boldsymbol{x_{ij}} = (\boldsymbol{x}_i^{Tx} + \boldsymbol{x}_j^{Rx})/2, \tag{2.8}$$

for $i = 1,...,M_t$ and $j = 1,...,M_r$. Presented in fig. 2.6 is a MIMO-setup with its corresponding virtual

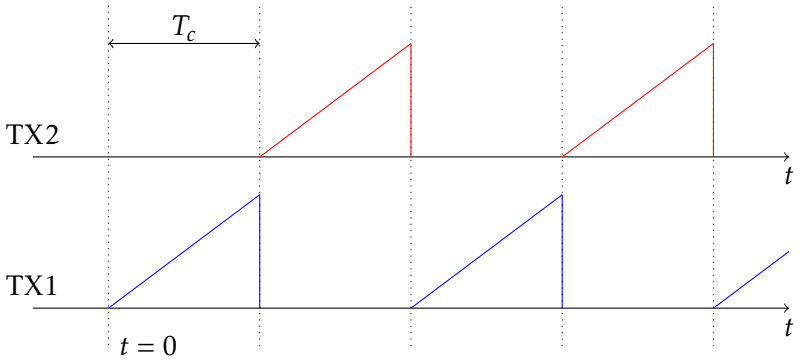

Figure 2.3.: Time division multiplexing for MIMO-radar.

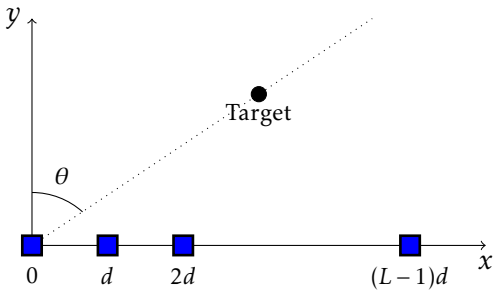

Figure 2.4.: Uniform Linear Array (ULA).

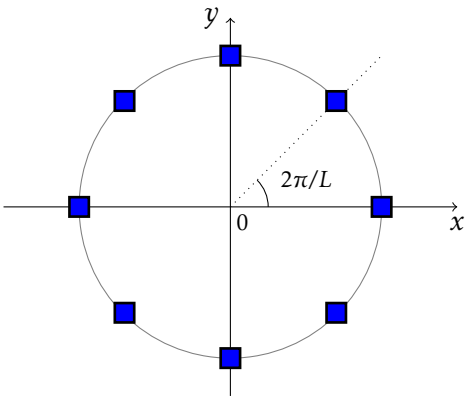

Figure 2.5.: Uniform Circular Array (UCA).

elements. Note that for this work the TX and RX elements are aligned in the vertical axis. This has been ignored here for better illustration.

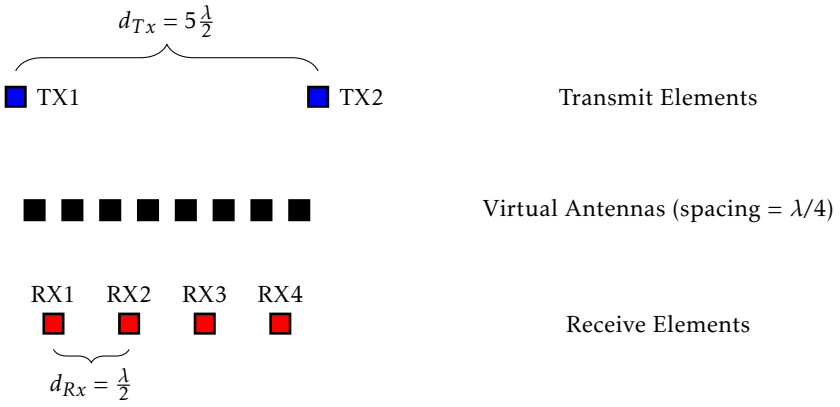

Figure 2.6.: MIMO-array

Under the described conditions the signal propagation path from a given TX element to a scatterer at point $\boldsymbol{p}$, plus the reflection path back to an RX element can be approximated as

$$P_{ij}(p) = |\boldsymbol{p} - \boldsymbol{x}_i^{Tx}| + |\boldsymbol{p} - \boldsymbol{x}_j^{Rx}| \approx 2|\boldsymbol{p} - \boldsymbol{x}_{ij}|. \tag{2.9}$$

2.3. Signal Model

For the following analyses a Frequency-Modulated Continuous-Wave (FMCW) signal model is taken into consideration. As the name indicates, the FMCW radar transmits a signal continuously, from which the frequency is increased with time. For MIMO radars, as explained before, the antennas do not transmit continuously given that they are switched after each cycle. For a linear increase of the frequency, the FMCW-chirp signal transmitted by each of the TX elements can be modeled as

$$s_T(t) = \exp[\mathrm{j}(2\pi f_c t + \pi k t^2)], \tag{2.10}$$

for $-T_c/2 \leq t \leq T_c/2$, where T_c is the chirp duration, f_c the carrier frequency and the chirp rate k is defined by

$$k = \pm B/T_c. \tag{2.11}$$

Under far-field conditions, the return echo caused by an object located ar rang R and an angle of θ with respect to the boresight, i.e. $(x, y) = (R\cos\theta, R\sin\theta)$, can be simplified to

$$\Delta t_{ij} = \frac{2R}{c} + \frac{2x_{ij}\sin\theta}{c}, \tag{2.12}$$

for the virtual element obtained from the i-th TX element and j-th RX element. The received signal results in

$$s_R(t) = A s_t(t - \Delta t_{ij}), \tag{2.13}$$

where the dependency of $s_R(t) = s_R^{ij}(t)$ on i and j has been omitted for clear notation.

Once the signal is received, it is down-converted in a pre-processing step by multiplying it with a replica of the transmitted signal. The outcome of the multiplication results in a component at intermediate frequency (IF) frequency, and an undesired component at a higher frequency. After low-pass filtering, the processed signal is

$$u_{ij}(t) = s_R^* s_T(t) = A\exp[\mathrm{j}(2\pi k \Delta t_{ij} t - \pi k \Delta t_{ij}^2 + 2\pi f_c \Delta t_{ij})]. \tag{2.14}$$

The sampled form of the IF signal given N samples can be expressed as

$$u_{ij}[n] = A\exp[\mathrm{j}(\phi + 2\pi \Psi_R n)], \tag{2.15}$$

where $\Psi_R = k\Delta t_{ij}\frac{T_c}{N}$ is the normalized frequency containing the range information and $\phi = -\pi k \Delta t_{ij}^2 + 2\pi f_c \Delta t_{ij}$ contains the phase information. This expression can be generalized to MIMO radar for the k-th observation interval by

$$u_k[n, n_C, n_A] = \sum_{m=0}^{M} A_m \exp[\mathrm{j}2\pi(\phi_m + \Psi_{R,m} n + \Psi_{D,m} n_C + \Psi_{\theta,m} n_A)] + w[n, n_C, n_A], \tag{2.16}$$

where $\Psi_D = \frac{2T_c f_0}{c_0} v_R$ and $\Psi_\theta = \sin(\theta)/2$ are the normalized frequencies containing the information about range-rate and azimuth. Moreover, $w[n, n_C, n_A]$ is the present additive white Gaussian measurement noise. The parameters n, n_C and n_A represent which sample, chirp, and antenna is being taken into account. Please note that ϕ_m does not correspond to ϕ.

The information collected from eq. (2.16) is usually arranged into a three-dimensional data cube as presented in fig. 2.7. Each of the dimensions correspond to a certain parameter that has to be estimated. The first dimension, contains the N samples of a pulse. This information corresponds to

the range estimation (**??**). The second dimension, stores the signal received by the each of the virtual elements for the same pulse. A variety of algorithms exists to process the data in this dimension and obtain and estimate for the azimuth profile (Section 2.5). Finally, the third dimension, contains multiple pulses. In other words, for a single virtual channel and range bin, the third dimension contains the received signal each time the cycle of pulses being transmitted restarts, i.e. each $T_c N_t$ seconds.

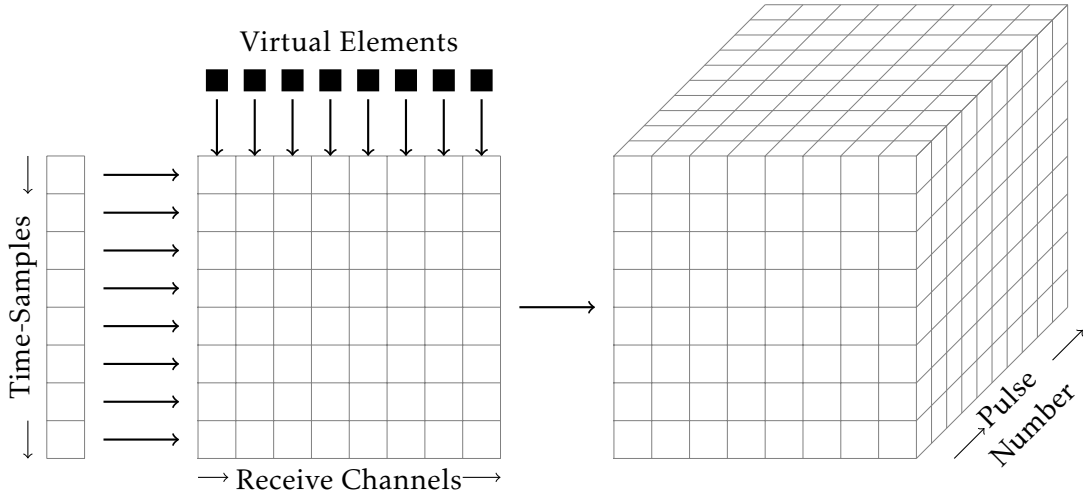

Figure 2.7.: Data Cube

In order to estimate the spectrum of the received signal and so to determine the unknown parameters R, v_R and θ for a given target, usually a three-dimensional Fast Fourier Transform (FFT) is applied to de IF signal

$$\hat{P}_k(\Psi_R, \Psi_D \Psi_\theta) = \sum_n \sum_{n_C} \sum_{n_A} a_R[n] a_D[n_C] a_\theta[n_A] u_k[n, n_A, n_C] \times \exp(-\mathrm{j}2\pi\Psi_R n) \exp(-\mathrm{j}2\pi\Psi_D n_C) \exp(-\mathrm{j}2\pi\Psi_\theta n_A), \quad (2.17)$$

$$\hat{P}_k(\Psi_R, \Psi_D) = \sum_n \sum_{n_C} \sum_{n_A} a_R[n] a_D[n_C] u_k[n, n_A, n_C] \times \exp(-\mathrm{j}2\pi\Psi_R n) \exp(-\mathrm{j}2\pi\Psi_D n_C), \quad (2.18)$$

however, this usually results in a bad estimation for the azimuth range. Specifics of the signal processing will be described in the following sections.

2.4. Range and Range-Rate Estimation

The estimation of the range and the range rate can be done by using a two-dimensional fft in the first and third dimension of the data cube.

$$\hat{P}_k(\Psi_R, \Psi_D) = \sum_n \sum_{n_C} a_R[n] a_D[n_C] u_k[n, n_A, n_C] \times \exp(-\mathrm{j}2\pi\Psi_R n) \exp(-\mathrm{j}2\pi\Psi_D n_C), \quad (2.19)$$

That's all for now, but what about Space- Adaptive Time Processing? WORK IN PROGRESS

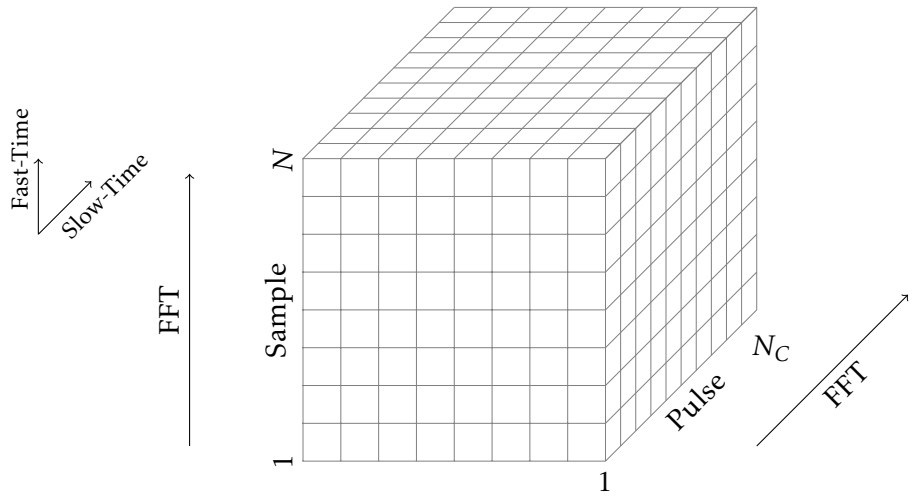

Figure 2.8.: CHANGE TO ILLUSTRATE DATA PROCESSING

2.5. Azimuth Estimation

Further definitions, for an antenna array the measured vector at time step t can be obtained by

$$\boldsymbol{x}(t) = \boldsymbol{a}(\theta)s(t), \tag{2.20}$$

where $s(t)$ is the received waveform, $\boldsymbol{x}(t)$ the value observed at the virtual elements and $\boldsymbol{a}(\theta)$ are called the steering vectors. The vector $\boldsymbol{x}(t)$ thus, can be expressed by

$$\boldsymbol{x}(t) = \begin{bmatrix} x_1(t) & x_2(t) & \dots & x_L(t) \end{bmatrix}^T \tag{2.21}$$

where L is the number of virtual elements. The steering vector depends on the arrangement of the radar array, for ULA it can be written as

$$\boldsymbol{a}_{ULA}(\theta) = \begin{bmatrix} 1 & e^{-\mathrm{j}kd\cos\theta} & \dots & e^{-\mathrm{j}(L-1)kd\cos\theta} \end{bmatrix} \tag{2.22}$$

where d is the separation between virtual elements. Assuming that M point scatterers are present in the measurement space, the received signal results in

$$\boldsymbol{x}(t) = \sum_{m=1}^{M} \boldsymbol{a}(\theta_m)s_m(t), \tag{2.23}$$

which can be expressed by the matrix notation

$$\boldsymbol{x}(t) = \mathbf{A}(\theta)\boldsymbol{s}(t) + \boldsymbol{n}(t), \tag{2.24}$$

where

$$\mathbf{A}(\theta) = \begin{bmatrix} \boldsymbol{a}(\theta_1) & \dots & \boldsymbol{a}(\theta_M) \end{bmatrix} \tag{2.25}$$

and

$$\boldsymbol{s}(t) = \begin{bmatrix} s_1(t) & \dots & s_M(t) \end{bmatrix}^T \tag{2.26}$$

and $\boldsymbol{n}(t)$ is additive white Gaussian noise. We further define the spatial covariance matrix as

$$\mathbf{R} = \mathbf{E}\left\{\boldsymbol{x}(t)\boldsymbol{x}^H(t)\right\} = \mathbf{A}\mathbf{E}\left\{\boldsymbol{s}(t)\boldsymbol{s}^H(t)\right\} + \mathbf{E}\left\{\boldsymbol{n}(t)\boldsymbol{n}^H(t)\right\} \tag{2.27}$$

where we further define

$$\mathbf{E}\left\{\boldsymbol{s}(t)\boldsymbol{s}^H(t)\right\} = \mathbf{P}. \tag{2.28}$$

and

$$\mathbf{E}\left\{\boldsymbol{n}(t)\boldsymbol{n}^H(t)\right\} = \sigma^2\boldsymbol{I}. \tag{2.29}$$

The $\mathbf{R}$ can then be decomposed in to

$$\mathbf{R} = \mathbf{APA}^H + \sigma^2\mathbf{I} = \mathbf{U}\Lambda\mathbf{U}. \tag{2.30}$$

where $\mathbf{U}$ is unitary and $\Lambda = \text{diag}\{\lambda_1, \lambda_2, ..., \lambda_L\}$ contains the eigenvalues ordered such as $\lambda_1 \geq \lambda_2 \geq ... \geq \lambda_L$ A further partition is made

$$\mathbf{R} = \mathbf{U}_s\Lambda_s\mathbf{U}_s^H + \mathbf{U}_n\Lambda_n\mathbf{U}_n^H \tag{2.31}$$

and the projectors are defined

$$\Pi = \mathbf{U}_s\mathbf{U}_s^H = \mathbf{A}(\mathbf{A}^H\mathbf{A})^{-1}\mathbf{A}^H \tag{2.32}$$

$$\Pi^\perp = \mathbf{U}_n\mathbf{U}_n^H = \mathbf{I} - \mathbf{A}(\mathbf{A}^H\mathbf{A})^{-1}\mathbf{A}^H \tag{2.33}$$

2.5.1. Conventional Beamforming

Problem of maximizing the output power, formulation

$$\max_{\boldsymbol{w}} \mathbf{E}\left\{\boldsymbol{w}^H\boldsymbol{x}(t)\boldsymbol{x}^H(t)\boldsymbol{w}\right\} = \max_{\boldsymbol{w}}\left\{\mathbf{E}|s(t)|^2|\boldsymbol{w}^H\boldsymbol{a}(\theta)|^2 + \sigma^2|\boldsymbol{w}|^2\right\}, \tag{2.34}$$

the solution is

$$\boldsymbol{w}_{BF} = \frac{\boldsymbol{a}(\theta)}{\sqrt{\boldsymbol{a}^H(\theta)\boldsymbol{a}(\theta)}} \tag{2.35}$$

so that the spatial spectrum can be expressed as

$$P_{BF}(\theta)\frac{\boldsymbol{a}^H(\theta)\mathbf{R}\boldsymbol{a}(\theta)}{\boldsymbol{a}^H(\theta)\boldsymbol{a}(\theta)} \tag{2.36}$$

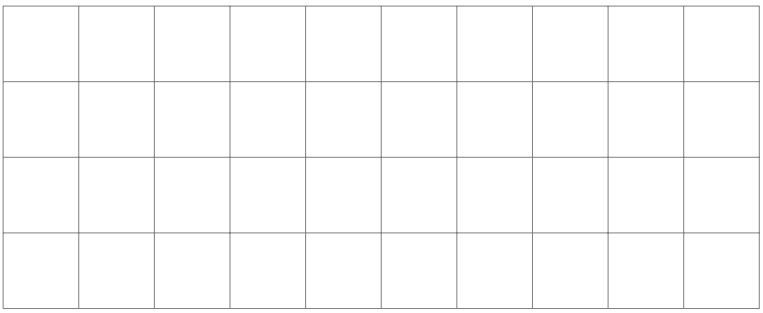

Figure 2.9.: We do need some kind of real result.

2.5.2. The MUSIC-algorithm

Based on the previous decomposition, the MUSIC algorithm takes advantage of the fact that the eigenvector in $\mathbf{U}_n$ are orthogonal to the steering matrix $\mathbf{A}$, i.e

$$\mathbf{U}_n^H \boldsymbol{a}(\theta) = 0, \quad \theta \in \{\theta_1, ..., \theta_M\} \tag{2.37}$$

The MUSIC "spatial spectrum" is defined as

$$P_M(\theta) = \frac{\boldsymbol{a}^H(\theta)\boldsymbol{a}(\theta)}{\boldsymbol{a}^H(\theta)\Pi^{\perp}\boldsymbol{a}(\theta)} \tag{2.38}$$

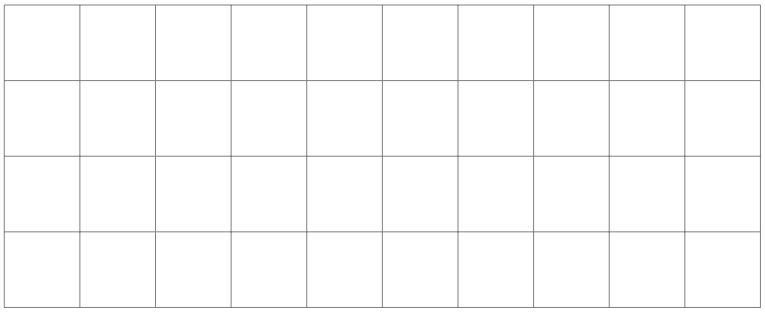

Figure 2.10.: We do need some kind of another real result.

3. Clustering

Note: At the moment it is not clear whether other clustering algorithms which are not density-based decompositions will be considered.

3.1. Density-Based Clustering

Density-based clustering algorithms have been developed in the context of data mining in big data bases and knowledge discovery. For radar applications, density-based clustering is of advantage since it is very efficient in a dynamic environment where insertions and deletions are present. Furthermore, no cluster-prototype has to be specified, i.e. the clusters can be of arbitrary shape. Last but not least, the number of clusters does not have to be known in advance, which is a disadvantage that most clustering algorithms present which make them unsuitable for radar-applications.

In section 3.1.1 some mathematical definitions that describe the way density-based clustering works are presented. Furthermore, section 3.1.2 presents the density-based spatial clustering of applicatios with noise (DBSCAN) algorithm.

3.1.1. Definitions

The key idea of density-based clustering is that for most points of a cluster, the ε-neighborhood for some $\varepsilon > 0$, has to contain at least a minimum numbber of points. In other words, the neighborhood has to exceed a density-threshold to be considered a cluster.

We define a distance-based ε-neighborhood N_ε of an object o on a set of points D by

$$N_\varepsilon(o) = \{o' \in D || o - o'| \leq \varepsilon\} \tag{3.1}$$

Furthermore, an object $p \in D$ is called *directly density-reachable* from an object $q \in D$ if

1. $p \in N_\varepsilon(q)$
2. $size(N_\varepsilon(q)) > MinPts$

where $size()$ returns the number of points in an ε-neighborhood and $MinPts$ is the threshold that it has to meet to be considered a cluster. Morever, the object $p \in D$ is called *density-reachable* from $q \in D$, if there is a chain of objects p_1,..., p_n, with $p_1 = q$ and $p_n = p$ such that for all $i = 1,..,n-1$: p_{i+1} is directly density-reachable o p_i. These definitions are illustrated in fig. 3.1

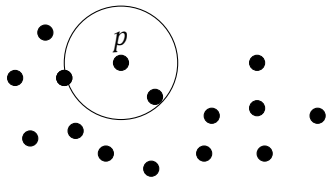

Figure 3.1.: Density-reachable example

Finally, an object p is density connected to an object q if there exist an object o such that both p and q are density-reachable from o, such as shown in fig. 3.2.Note that all these properties are dependent on ε and $MinPts$. In literature, for instance, it would be said that an object is density connected to another object with respect to ε and $MinPts$, however this statement has been omitted since it is implied.

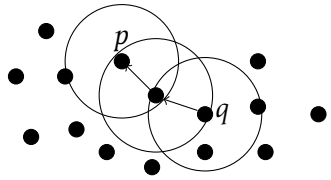

Figure 3.2.: Density-reachable example

With the previous definitions, one can now define the concepts of a *density-conenected set*, which is a subset C of a database D that satisfies the following conditions

1. Maximality: For all p,$q \in D$: if $p \in C$ and q is density-reachable from p, then $q \in C$.
2. Connectivity: For all p,$q \in C$: p is density-connected to q.

Now, one can define how a database should be decomposed after the clustering algorithms have been applied. The result is called density-based-decomposition (DBD) and should meet the following conditions

1. $DBD = \{S_1, ..., S_, N\}, k \geq 0$
2. $S_1 \cup ... \cup S_k \cup = D$
3. For all $i \leq k$: S_i is a *density-connected* set
4. If there exists a *density-connected* set $S \in D$, then there exists an $i \leq k$ so that $S = S_i$
5. $N = D \setminus (S_1 \cup ... \cup S_k)$ is called the noise with respect to the decomposition DBD.

This decomposition should be the output of the clustering algorithms where the subsets S_i are the clusters and N are any detections that were not assigned to any cluster.

3.1.2. DBSCAN

In this section, a MATLAB version of the DBSCAN is presented and explained.

```
%include matlab code
```

4. Multi-Target Tracking

After a correct detection and clustering of targets, the detections have to be assigned to tracks which are to be updated over time. In this case, it is done to create a history of each of the target's range, azimuth angle and Doppler velocity. In a further step, the Micro-Doppler signature can be extracted from each of the tracks and be used as an input for the classifiers. More over, by keeping track of the measurements corresponding to each track, one can produce an estimate of future positions of the target, which result into a more accurate measurement of the targets position. This process is called Multi-Target Tracking (MTT).

Each track of a MTT-algorithm contains a Kalman Filter (section 4.2) which is a commonly used filter to predict future states and to calculate variables that cannot be measured directly. At each step, gating (section 4.3) is applied to each of the new detections to reduce the scope of detections that can be assigned to a given track at each time step k. After gating, the detections calculated in a given step are assigned to each of the tracks. For this, the assignment problem has to be solved (section 4.4). After the assignment has been done, the state of each of the tracks is updated according to pre-established rules (section 4.5). The whole process used for the MTT is illustrated in fig. 4.1. Given that usually a constant-velocity model is assumed, a special model needs to be

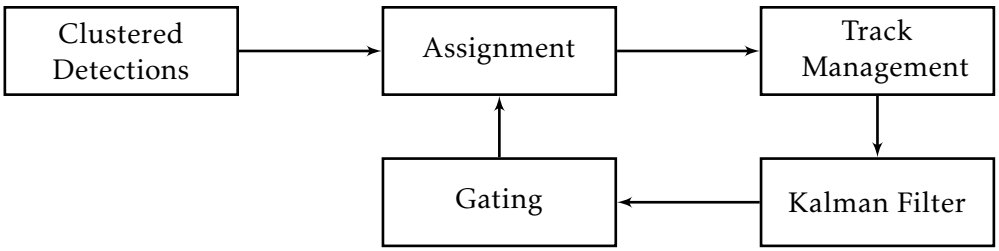

Figure 4.1.: MTT-process

implemented to consider the cases where the target has an (unknown) acceleration. This is issue is handled in section 4.6.

4.1. State Variable Representation of an LTI System

A Linear Time Invariant (LTI) system can be described by by three variables, input, output and the state variable. In the case of radar, the state can be design to contain several attributes of single targets measured by the radar such as range, range-rate and azimuth angle. Since we desire to determines a target's position and velocity in Cartesian coordinates, the state vector

$$\boldsymbol{x} = \begin{bmatrix} x \\ y \\ v_x \\ v_y \end{bmatrix}, \tag{4.1}$$

has been chosen. The continuous-time linear system can then be written as

$$\dot{\boldsymbol{x}}(t) = \mathbf{A}(t)\boldsymbol{x}(t) + \mathbf{B}(t)\boldsymbol{u}(t) + \tilde{\boldsymbol{v}}(t), \tag{4.2}$$

where t represents time and

$\boldsymbol{x}$	is the state vector of dimension n_x and $\dot{\boldsymbol{x}}$ its time derivative.
$\boldsymbol{u}$	is the input(or control) vector of dimension n_u
$\tilde{\boldsymbol{v}}$	is the process noise
A,B	are known matrices of dimensions $n_x \times n_x$ and $n_x \times n_u$

The output of the system can be represented by

$$\boldsymbol{z}(t) = \mathbf{C}(t)\boldsymbol{x}(t) + \tilde{\boldsymbol{w}}(t), \tag{4.3}$$

where

$\boldsymbol{z}$	is the output vector of dimension n_z
$\tilde{\boldsymbol{w}}$	the output disturbance, or measurement noise and
C	is a known matrix od dimension $n_z \times n_x$

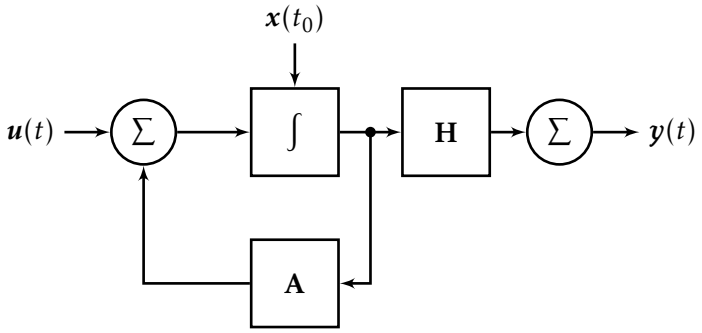

Figure 4.2.: An LTI System

Such an LTI system is depicted in fig. 4.2. Given the initial condition $\boldsymbol{x}(t_0)$, a solution to eq. (4.2) can be found as

$$\boldsymbol{x}(t) = \Phi(t - t_0)\boldsymbol{x}(t_0) + \int_{t_0}^{t} \Phi(t - \tau)\mathbf{B}(\tau)\boldsymbol{u}(\tau)\,\mathrm{d}\tau. \tag{4.4}$$

In the case of radar tracking, however, one only obtains detection at discrete time-steps. Thus, a discrete-time representation of the LTI system is to be found

$$\boldsymbol{x}[n+1] = \mathbf{A}[n]\boldsymbol{x}[n] + \mathbf{B}[n]\boldsymbol{u}[n] + \boldsymbol{v}[n] \tag{4.5}$$

$$\boldsymbol{z}[n] = \mathbf{H}[n]\boldsymbol{x}[n] + \boldsymbol{w}[n] \tag{4.6}$$

The state transition matrix for our case is the so called Newtonian matrix

$$\Phi = \begin{bmatrix} 1 & 0 & T & 0 \\ 0 & 1 & 0 & T \\ 0 & 0 & 1 & 0 \\ 0 & 0 & 0 & 1 \end{bmatrix}. \tag{4.7}$$

4.2. The Kalman Filter

Different classes of filters (or estimators) have been used for tracking. One of the simplest class of these filters is, for instance, are the so called "Fixed-Coefficient" filters. The most implemented of these are the $\alpha\beta$ and $\alpha\beta\gamma$ trackers [cite]. These filter provide smoothed and predicted data for target position, velocity and in case of the latter, acceleration. Nonetheless, given the better estimates it provides, the Kalman filter has been implemented primarily for radar-tracking purposes. Additionaly, the Kalman filter presents the following advantages over the Fixed-Coefficient filters.

1. The gain coefficients are computed dynamically, i.e. the same filter can be used for targets of different nature
2. The filter is robust against missed detections
3. Provides an accurate measure of the covariance matrix, which is relevant for gating and association processes

An overview of the process undertaken by the Kalman filter is presented in fig. 4.3. Before pre-

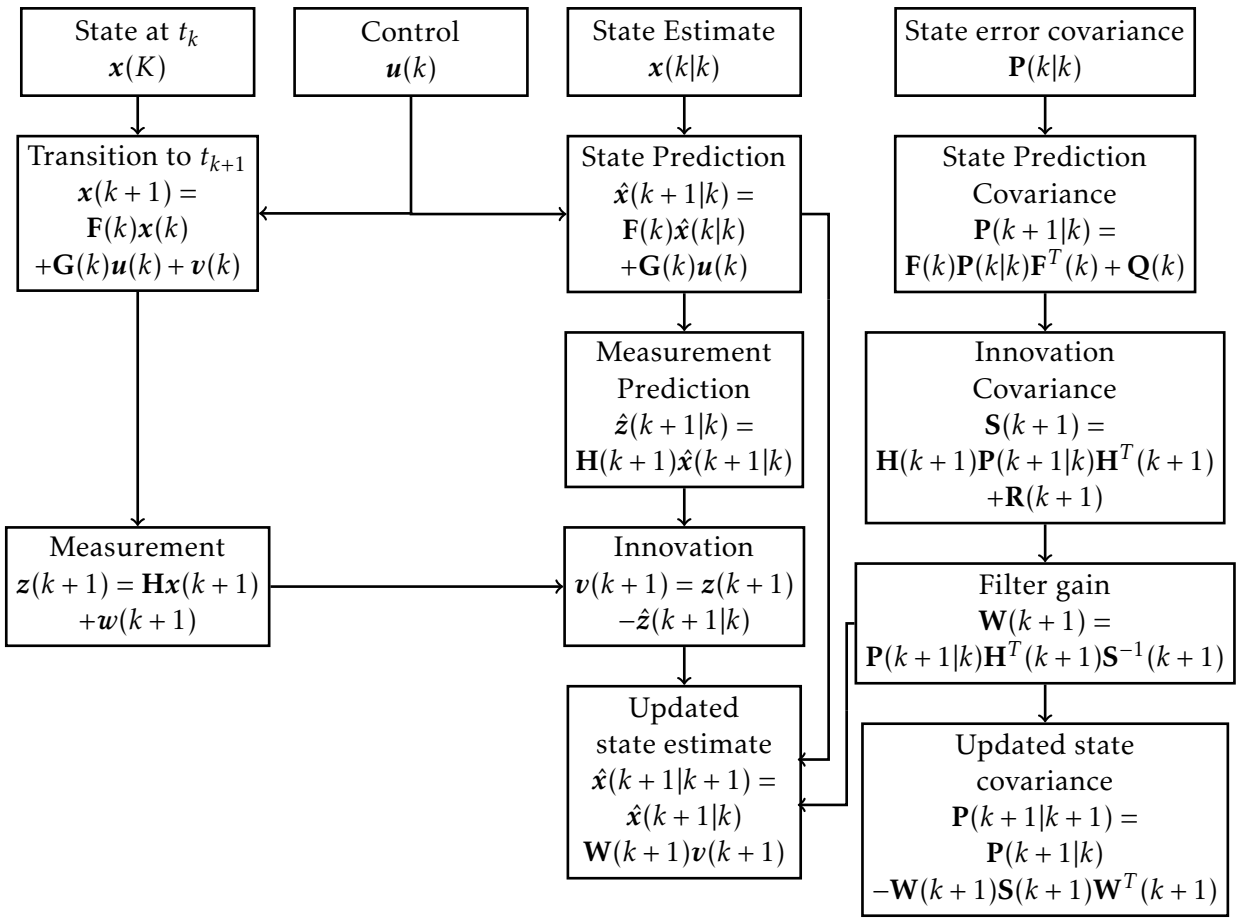

Figure 4.3.: The Kalman Filter

senting the equations that describe the Kalman filter, the notation is introduced. $\hat{\boldsymbol{x}}(n|m)$ represents the estimate during the n-th sampling interval using all data up to the m-th sampling interval, and $z(n)$ contains the measurements (or detections that have been assigned to the corresponding track) obtained at the n-th time-step.

4.2.1. Estimation in Linear Systems

The filtering equation is given by

$$\boldsymbol{x}(n|n) = \boldsymbol{x}_s(n) = \boldsymbol{x}(n|n-1) + \mathbf{W}(n)\boldsymbol{v}(n), \tag{4.8}$$

where

$\boldsymbol{x}_s(n)$ is the smoothed output of the Kalman filter

$\mathbf{W}(n)$ are the dynamically computed filter gains

$\boldsymbol{v}(n)$ is the innovation vector

The innovation vector contains information about how much the estimate $\boldsymbol{x}(n|n-1)$ differs from the newly obtained measurements $y(n)$ and can be written as

$$\boldsymbol{v}(n) = \boldsymbol{y}(n) - \mathbf{H}\boldsymbol{x}(n|n-1), \tag{4.9}$$

where $\mathbf{H}$ is called the observation matrix. In our case, the measurement vector has the form

$$\boldsymbol{y}(n) = \begin{bmatrix} x_m(n) \\ y_m(n) \end{bmatrix}, \tag{4.10}$$

so that $\boldsymbol{v}(n)$ only represent the innovation in the position measurements. Therefore, the observation matrix results in

$$\mathbf{H} = \begin{bmatrix} 1 & 1 & 0 & 0 \end{bmatrix}. \tag{4.11}$$

The filter gains are computed at each time step by

$$\mathbf{W}(n+1) = \mathbf{P}(n+1|n)\mathbf{H}^T\mathbf{S}^{-1}(n+1) \tag{4.12}$$

where

$\mathbf{P}$ represents the predictor covariance matrix and,

$\mathbf{S}$ the measurement prediction covariance.

The state prediction covariance is first calculated recursively by

$$\mathbf{P}(n|n+1) = \mathbf{E}\{\boldsymbol{x}_s(n+1)\boldsymbol{x}_s^*\} = \mathbf{A}\mathbf{P}(n|n)\mathbf{A}^T + \boldsymbol{Q}, \tag{4.13}$$

where $\boldsymbol{Q}$ is the covariance matrix for the input $\boldsymbol{u}(n)$. After the filter gains have been calculated by eq. (4.12), the state covariance is updated by

$$\mathbf{P}(n+1|n+1) = \mathbf{P}(n+1|n) - \mathbf{W}(n+1)\mathbf{S}(n+1)\mathbf{W}^T(n+1). \tag{4.14}$$

The innovation covariance, or measurement prediction covariance is given by

$$\mathbf{S}(n+1) = \mathbf{H}\mathbf{P}(n+1|n)\mathbf{H}^T + \mathbf{R}, \tag{4.15}$$

where $\mathbf{R}$ is the measurement covariance.

4.2.2. Initialization of State Estimators

When a detection that has not been assigned to an existing track is present, a tentative track is initiated (see section 4.5) the Kalman filter is initialized. First, the state vector as

$$\boldsymbol{x}(0) = \begin{bmatrix} r_m \cos(\theta_m) \\ r_m \sin(\theta_m) \\ 0 \\ 0 \end{bmatrix}, \tag{4.16}$$

where r_m and θ_m are the measured range and azimuth respectively. Given that the measurement of the azimuth angle is not very accurate, we have chosen to initialize the velocities v_x and v_y of each target with $v_x = 0$ and $v_y = 0$. Note that, however, the velocities can also be initialized by taking two position measurements and calculating

$$v_x = \frac{x_m(0) - x_m(-1)}{\Delta} \qquad v_y = \frac{y_m(0) - y_m(-1)}{\Delta} \tag{4.17}$$

where Δ is the time between measurements, $x_m(n) = r_m(n)\cos(\theta_m(n))$ and $y_m(n) = r_m(n)\sin(\theta_m(n))$. Furthermore, the initial covariance matrix is calculated depending on the measurement matrix

$$\mathbf{R} = \begin{bmatrix} R_{11} & R_{12} \\ R_{21} & R_{22} \end{bmatrix} \tag{4.18}$$

as

$$\mathbf{P}(0|0) = \begin{bmatrix} R_{11} & R_{12} & R_{11}/\Delta & R_{12}/\Delta \\ R_{21} & R_{22} & R_{21}/\Delta & R_{22}/\Delta \\ R_{11}/\Delta & R_{12}/\Delta & 2R_{11}/\Delta^2 & 2R_{12}/\Delta^2 \\ R_{22}/\Delta & R_{22}/\Delta & 2R_{21}/\Delta^2 & 2R_{22}/\Delta^2 \end{bmatrix} \tag{4.19}$$

TO DO (IN RESEARCH TOO): Choosing appropiate **R** and **Q** matrices

4.3. Gating Techniques

Gating is a technique used to eliminate extremely unlikely observation-to-track pairings. A gate is calculated around the output of the Kalman filter (predicted position), and any observation outside of this gate is not further consider for that track. Furthermore if only one observation is found within the gate, then the observation is assigned directly to that track and no further processing is required (see section 4.4).

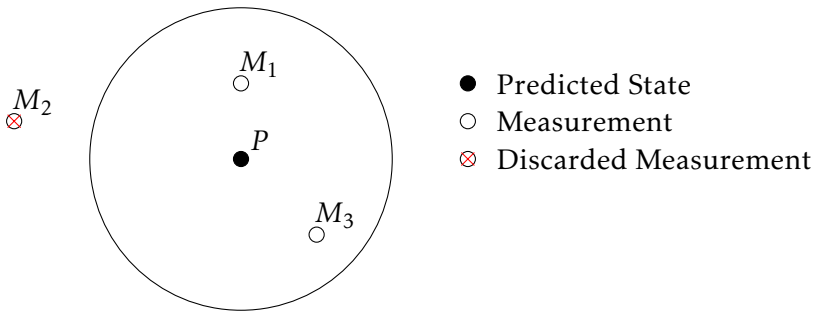

Figure 4.4.: Gating

One of the simplest gating techniques is using rectangular gates. A given observation is also said to satisfy the gates of a given track if the all the elements of the innovation vector satisfy

$$|\boldsymbol{v}(n)| \leq K_G \sigma_r \tag{4.20}$$

where σ_r is the residual standard deviation that can be expressed in terms of measurement σ_o^2 and prediction σ_p^2

$$\sigma_r = \sqrt{\sigma_o^2 + \sigma_p^2}. \tag{4.21}$$

Note that the values σ_o and σ_p can be found in the Kalman filter equations as

$$\sigma_o = R_{11} \qquad \sigma_p = P_{11} \tag{4.22}$$

The constant K_G can be chosen freely. Usually, a Gaussian error model is assumed to that choosing $K_G = 3$ leads to the probability of a valid observation satisfying the gating test to be about 99 percent.

4.4. The Assignment Problem

In a dense target environment, the gating technique is not sufficient enough to discriminate between detections. Thus a further assignment logic has to be implemented. Conflicts can occur for instance, when a detection satisfies the gating of different tracks, or when a track was multiple detections within its gate. This problem is called the assignment problem.

There are basically two types of solutions. The nearest-neighbor (NN)-approach (section 4.4.1) and the "all-neighbors" approach (section 4.4.2 and section 4.4.3). The first step of all solutions, however, is the same. First, an assignment matrix is built. For this, the norm of the innovation vector that would result if track i and detection j would be assigned is defined as

$$d_{ij}^2 \triangleq \boldsymbol{v}_{ij}(n)^T \mathbf{S}_i^{-1}(n) \boldsymbol{v}_{ij}(n), \tag{4.23}$$

where $\mathbf{S}_i(n)$ is the residual covariance matrix defined in eq. (4.15). Furthermore, it is assumed that the residual has a Gaussian distribution

$$g_{ij} = \frac{\exp(-\frac{d_{ij}^2}{2})}{(2\pi)^{M/2}\sqrt{|\mathbf{S}_i|}}, \tag{4.24}$$

where M is the measurement dimension and $|\mathbf{S}_i|$ the determinant of $\mathbf{S}_i$.

The basic goal is to make assignment decisions based on the maximization of g_{ij}, which is equivalent to minimizing the quantity

$$d_{Gij}^2 = d_{ij}^2 + \ln|\mathbf{S}_i|, \tag{4.25}$$

which will be used as distance function for use in the assignment problem.

4.4.1. NN-approach

For the NN approach, first an assignment matrix as the one depicted in table 4.1 is built. Observations that are know within the gate of a certain track, will be identified as X. Otherwise, the distance function of of the corresponding observation and track is calculated.

There are different ways to solve the assignment problem from the assignment matrix following a NN-approach.Two suboptimal solutions are presented and (LATER: OPTIMAL SOLUTION).

Suboptimal Solution one:

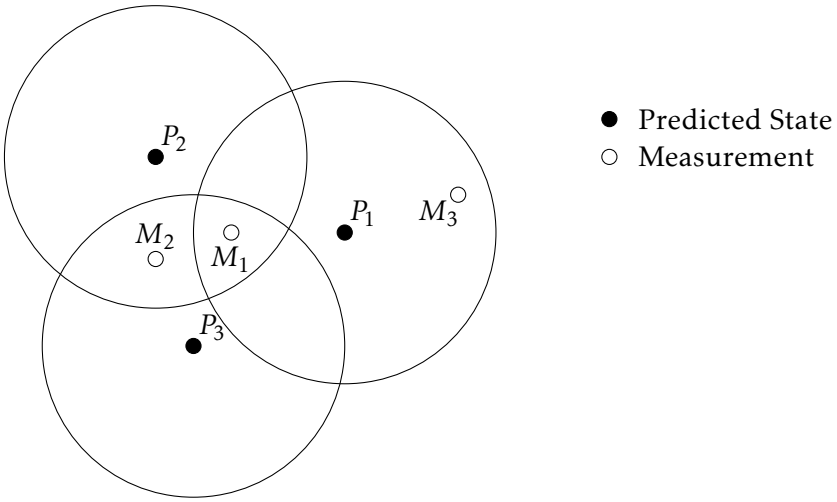

Figure 4.5.: Example of conflict situations for assignment

1. Observations that are considered for singly-validated tracks will not be considered for mutiply-validated tracks.

2. Observations that are in multiple tracks will not be considered for tracks that contain single-validated observations

3. Repeat 1. and 2. until the assignment matrix is not changed anymore

4. For the remaining tracks with multiple observations, select the observation with minimum distance

5. For the remaining observations that validate with various tracks, assign to th track with the minimum distance

Suboptimal Solution two:

1. Search the matrix for the minimum distance observation-to-track pair and assign it

2. Remove the assigned pair from the matrix and repeat 1. until all possible assignments have been made.

4.4.2. PDA-approach

4.4.3. JPDA-approach

4.5. Track Life Stages

NOTE: For now very simple methods for track management have been implemented:
Track Initiaiton: Any detection not assigned Track Confirmation: If a tentative track has at least 3 detections for 5 time steps Track Deletion: After 10 consecuitive missed detections

M / P	M_1	M_2	M_3
P_1	x	x	x
P_2	x	x	x
P_3	x	x	x

Table 4.1.: Assignment matrix example

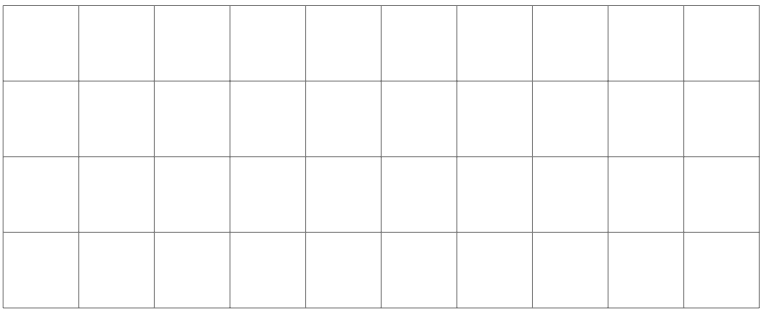

Figure 4.6.: Density-reachable example

4.5.1. Track Confirmation

4.5.2. Track Deletion

4.6. Maneuver Detection and Adaptive Filtering

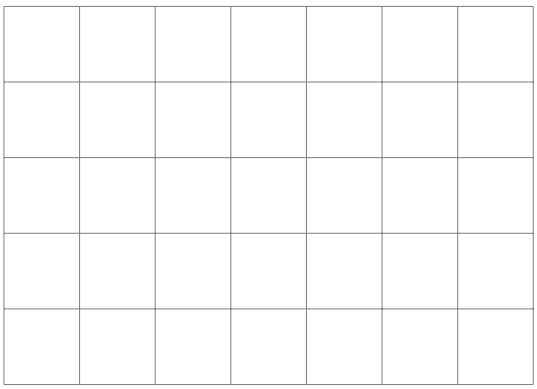

Figure 4.7.: A figure

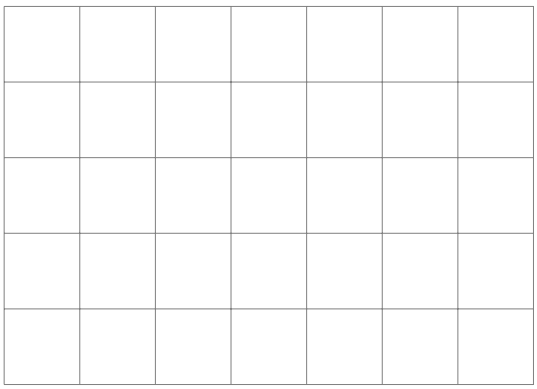

Figure 4.8.: Another figure

5. Feature Extraction

After a correct algorithm for multi-target tracking has been implemented, one has to generate an input for the classifiers, which are presented in chapter 6. Different characteristics of each of the tracks have been used in literature for classification for various purposes. An overview of the different features that have been used as an input for classifiers is presented in section 5.2. The possible selection of features is vast, however given the increase in computation each feature extraction one should select the features resulting in a more reliable classification. This is not straightforward, since the performance of each feature for classification is application-dependent. For each track j at time step k we first generate the n-tupel

$$\check{v}_j[k] = \left(\hat{\Psi}_{D,1}, \hat{\Psi}_{D,2}, \hat{\Psi}_{D,3}, ..., \hat{\Psi}_{D,L}\right), \tag{5.1}$$

containing the normalized range-rated obtained from all clusters contributing to the track. Other features are stored in n-tupels with elements corresponding to the ones in $\check{v}_j[k]$ as

$$\check{a}_j[k] = (\hat{a}_1, \hat{a}_2, \hat{a}_3, ..., \hat{a}_L). \tag{5.2}$$

Given that the purpose of this thesis is the classify objects according to their micro-Doppler spectrum, the micro-Doppler effect is explained in detail in section 5.1, and some measurement results presenting the micro-Doppler spectrum of pedestrians are given in section 5.3.

5.1. The Micro-Doppler Effect

As briefly explained in section 2.4, a target with a radial speed with respect to the radar will produce a frequency shift on the reflected signal called the Doppler shift. This frequency shift is due to the so-called bulk motion of the object, that is the general velocity at which an object is moving. For many types of targets, however, oscillatory motions, which can also be called *micro motions*, might be present. Examples of micro motions include a rotating propeller of an aircraft, a rotation antenna or the flapping wings of bird. For our scenario micro motions are found in the swinging of arms an legs of a pedestrians or the movement of the legs of a cyclist. For vehicles, the rotation of wheels could be considered a micro motion.

These micro motions cause for a further frequency shift in the transmitted signals called the *Micro-Doppler effect*[5]. For periodic vibrations or rotations, such as the case of the limbs of a pedestrian, shifts about the the center of the Doppler-shift due to the bulk motion are observed.

5.2. Overview of Features

The amount of features that have been used for classification in literature is vast [6, 7].

Cluster Related Features [8].

- Extent of Target
- Size of Clusters

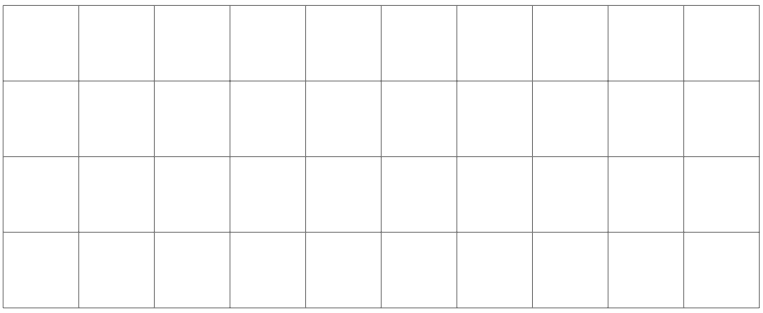

Figure 5.1.: Result to illustrate the Micro Doppler Effect

Kalman Filter Related Features [9]

- Matrix **K**
- Matrix **Q**

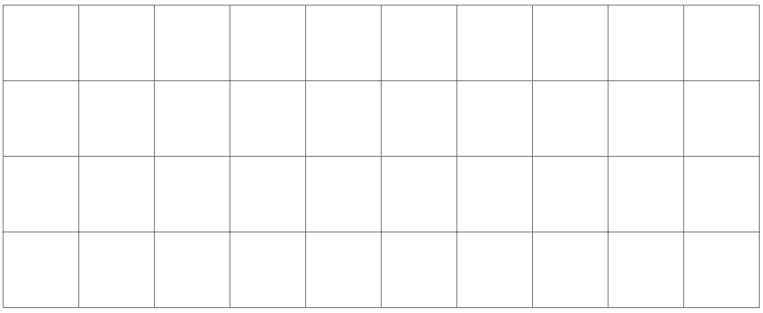

Figure 5.2.: Figure to illustrate how the matrices change for pedestrians vs. vehicles vs. bikes6

Doppler Effect Related Features [7].

- The total BW of the Doppler Signal
- The STD of the Doppler Signal
- The micro-Doppler Period
- The micro-Doppler Energy
- Envelope of the micro-Doppler Spectrum
- Doppler Offset
- The BW of the Doppler Signal without micro-Doppler

Features for classifying human-activities [6]

- The torso Doppler Frequency
- The period of the limb motion
- The bandwidth of torsco oscillations
- Limb acceleration and deceleration
- Maximum limb swing speed

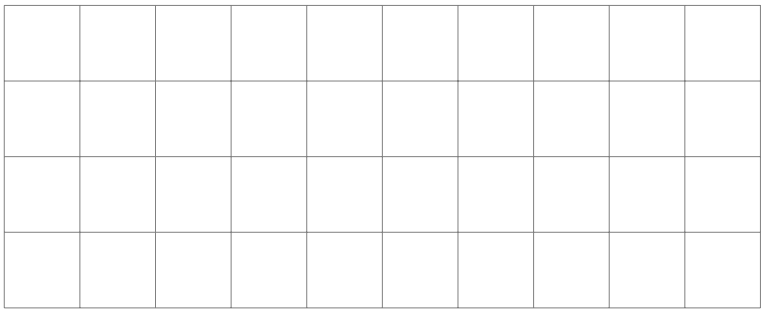

Figure 5.3.: Figure to illustrate the Doppler effect features

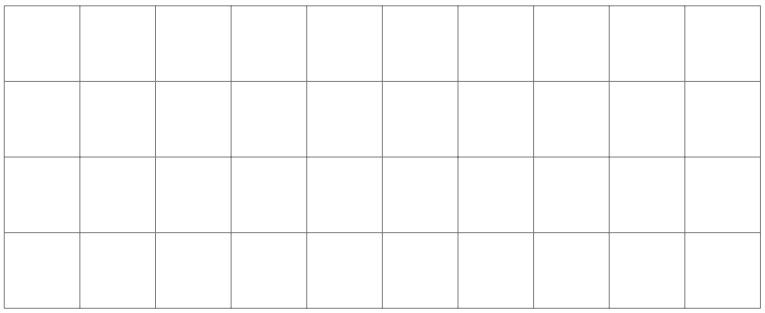

Figure 5.4.: Figure to illustrate the Doppler effect of human motion, maybe walking vs running

5.3. Results

6. Classification

6.1. Support Vector Machine

7. Results

8. Summary and Outlook

A. Symbols and Constants

General

$\oint$	Integration over a closed curve

Latin alphabet

B	Bandwith
f_0	Center Frequency
f_d	Doppler Frequency
f_r	Pulse Repetition Frequency (PRF)
R	Range
R_u	Unambiguous Range
T	Pulse Repetition Interval (PRI)
v	Target Velocity

Greek alphabet

ΔR	Range Resolution
ΔT	Delay
λ	wavelength
τ	Pulse Width

Constants

c_0	=	299729458 m/s

B. Mathematical Formulas

Bibliography

[1] Bassem R. Mahafza. *Radar Systems Analysis and Design Using MATLAB*. CRC Press, January 2002.

[2] E. Fishler, A. Haimovich, R. Blum, D. Chizhik, L. Cimini, and R. Valenzuela. MIMO radar: an idea whose time has come. In *Proceedings of the 2004 IEEE Radar Conference (IEEE Cat. No.04CH37509)*, pages 71–78, April 2004.

[3] Yanchuan Huang, Paul Victor Brennan, Dave Patrick, I. Weller, Peters Roberts, and K. Hughes. FMCW Based MIMO Imaging Radar for Maritime Navigation. *Progress In Electromagnetics Research*, 115:327–342, 2011.

[4] Xiaofei Zhang, Xin Gao, Gaopeng Feng, and Dazhuan Xu. Blind Joint DOA and Dod Estimation and Identifiability Results for MIMO Radar with Different Transmit / Receive Array Manifolds. *Progress In Electromagnetics Research B*, 18:101–119, 2009.

[5] Victor C. Chen. *The micro-Doppler effect in radar*. Artech House, 2011.

[6] Y. Kim and H. Ling. Human Activity Classification Based on Micro-Doppler Signatures Using a Support Vector Machine. *IEEE Transactions on Geoscience and Remote Sensing*, 47(5):1328–1337, May 2009.

[7] R. M. Narayanan and M. Zenaldin. Radar micro-Doppler signatures of various human activities. *Sonar Navigation IET Radar*, 9(9):1205–1215, 2015.

[8] E. Schubert, F. Meinl, M. Kunert, and W. Menzel. Clustering of high resolution automotive radar detections and subsequent feature extraction for classification of road users. In *2015 16th International Radar Symposium (IRS)*, pages 174–179, June 2015.

[9] S. Heuel and H. Rohling. Two-stage pedestrian classification in automotive radar systems. In *2011 12th International Radar Symposium (IRS)*, pages 477–484, September 2011.